Journal of Power Sources 188 (2009) 353–358

Contents lists available at ScienceDirect

Journal of Power Sources

journal homepage: www.elsevier.com/locate/jpowsour

Kinetics of oxygen reduction reaction on $Co_{rich\ core}$-$Pt_{rich\ shell}$/C electrocatalysts

Mei Hua Lee[a,b], Jing Shan Do[a,*]

[a] Department of Chemical and Materials Engineering, Tunghai University, Taichung 40704, Taiwan
[b] Department of Industrial Engineering and Management, Diwan College of Management, Tainan 72141, Taiwan

ARTICLE INFO

Article history:
Received 26 October 2008
Received in revised form 9 December 2008
Accepted 10 December 2008
Available online 24 December 2008

Keywords:
Kinetics
Rotating disk electrode
Oxygen reduction reaction
Core-shell electrocatalysts

ABSTRACT

The nanostructured $Co_{rich\ core}$-$Pt_{rich\ shell}$/C electrocatalysts were prepared by combining the thermal decomposition and the chemical reduction methods. The particle size of homemade $Co_{rich\ core}$-$Pt_{rich\ shell}$/C analyzed by TEM was significantly greater than that of Pt grain size calculated from the XRD data due to the existence of Co in core. The mass activity and specific activity of oxygen reduction reaction (ORR) at the overpotential (η) of 0.1 V were 6.69 A g^{-1} and 1.51×10^{-5} A cm^{-2} for Pt/C, and 10.22 A g^{-1} and 2.73×10^{-5} A cm^{-2} for $Co_{rich\ core}$-$Pt_{rich\ shell}$/C in 0.5 M $HClO_4$ aqueous solution at 25 °C. The Tafel slopes of ORR on Pt/C and $Co_{rich\ core}$-$Pt_{rich\ shell}$/C electrocatalysts were obtained as 64 and 67 mV dec^{-1} at a lower η (50–100 mV), and 116 and 110 mV dec^{-1} at a higher η (120–200 mV). The exchange current densities of ORR on Pt/C and $Co_{rich\ core}$-$Pt_{rich\ shell}$/C evaluated based on the higher Tafel slope regions were 6.76×10^{-5} and 9.21×10^{-5} A cm^{-2}, respectively. The experimental results indicated that the ORR on $Co_{rich\ core}$-$Pt_{rich\ shell}$/C electrocatalyst in 0.5 M $HClO_4$ aqueous solution was a four electron transfer mechanism and first order with respect to the dissolved oxygen.

1. Introduction

Compared with other power sources, the advantages of fuel cells are generally recognized with the characteristics of high energy efficiency and environment friendliness. However, the high cost of the Pt electrocatalysts is one of the main obstructions for commercializing fuel cells. Therefore, electrocatalysts used for fuel cells have been extensively studied aiming to improve catalytic activity at low cost. Developing cathodic catalysts with high electroactivity for oxygen reduction reaction (ORR) is one of the main challenges. Platinum and its alloys supported on carbon black are extensively used as the cathodic electrocatalysts because of the four-electron mechanism for reducing O_2 to H_2O in the low and medium temperature proton exchange membrane fuel cells (PEMFC) [1]. Using Pt-M alloys (M is the transition metals) as the cathodic electrocatalysts, the promotion in the ORR electroactivity is attributed to decreasing the Pt–Pt distance (geometric effect) and forming an electronic structure with higher 5*d* orbital vacancies, which led to an increase in π electron donation from O_2 to the Pt surface (electronic effect) [1]. Accordingly, the utility of Pt increases, and the amount of expensive Pt can be effectively decreased. Recently, Pt-Co alloys have been extensively developed as the cathodic electrocatalysts in PEMFC because of the significant enhancement in ORR on Pt-Co alloys [2–8].

The unfavorable effect of transition metal ions such as Fe^{3+}, Co^{2+}, and Ni^{2+} in the electrolyte, which simulates the dissolution of transition metal from the Pt-M alloys electrocatalysts, on the electroactivity of ORR have been demonstrated in the literatures [2,6–9]. One of the possible ways to overcome the dissolution of transition metals from Pt-M is to prepare the transition metals at the core and the Pt at the shell ($M_{rich\ core}$-$Pt_{rich\ shell}$) type of electrocatalyst. Using $M_{rich\ core}$-$Pt_{rich\ shell}$ as the electrocatalyst of ORR, the transition metal (M) at the core can be protected by the Pt at the shell, and the dissolution of transition metal and the decay of the electroactivity may be inhibited. The $Co_{rich\ core}$-$Pt_{rich\ shell}$/C designed and prepared as the cathodic electrocatalyst used for ORR was studied in our previous research [10].

In this study, the thermal decomposition of dicobalt octacarbinyl ($Co_2(CO)_8$) and the reduction of platinum acetylacetonate ($Pt(acac)_2$) in series were used to prepare $Co_{rich\ core}$-$Pt_{rich\ shell}$ on carbon powder (XC-72) ($Co_{rich\ core}$-$Pt_{rich\ shell}$/C). The properties of homemade electrocatalysts and the kinetics of ORR on the $Co_{rich\ core}$-$Pt_{rich\ shell}$/C, which was prepared on the rotating disk electrode, were also examined.

2. Experimental

The carbon support was pretreated by mixing 5 g carbon black (XC-72, Cabot) with 50 ml 65% HNO_3 aqueous solution and heated to 100 °C for 8 h. After filtration and washing with deionized (DI) water several times, the carbon black was dried in a vacuum oven at 70 °C for 24 h and used as the support for preparing electrocat-

* Corresponding author. Tel.: +886 4 23590262x114; fax: +886 4 2359009.
E-mail address: jsdo@thu.edu.tw (J.S. Do).

0378-7753/$ – see front matter © 2008 Elsevier B.V. All rights reserved.
doi:10.1016/j.jpowsour.2008.12.051

alysts. The solution of 60 mg $Co_2(CO)_8$ (95%, Acros) dissolved in 10 ml diphenyl ether (dpe, ≥98%, Merck) mixed with 100 mg carbon black was sparged with N_2 for 30 min, and then heated to 142 °C and refluxed in N_2 atmosphere for 30 min to prepare Co/C. Then, 50 mg platinum acetylacetonate ($Pt(acac)_2$, 98%, Strem), 100 mg 1, 2-hexadecanediol (90%, Aldrich), 56 μl oleic acid (65–68%, Merck), and 61.5 μl oleylamine (70%, Aldrich) were added and increased the temperature to 205 °C for 1 h to prepare Pt onto Co/C. The electrocatalyst was obtained by centrifuging (6000 rpm) and washing with ethanol several times, and then dried at a 100 °C vacuum oven for 24 h. The Pt/C was also prepared to get the similar Pt loading of $Co_{rich\ core}$-$Pt_{rich\ shell}$/C.

The morphologies of Pt/C and $Co_{rich\ core}$-$Pt_{rich\ shell}$/C were characterized by using transmission electron microscopy (TEM, JEOL JEM-1010) with an accelerating voltage of 120 kV. The crystal structure and grain size of the electrocatalysts were analyzed and evaluated by the X-ray diffractometer (XRD, SHIMADZU XRD-6000) with Cu Kα radiation (λ = 1.54 Å, 40 kV and 30 mA) over 2θ angle from 20 to 90° at a rate of 2° min^{-1}.

The electrochemical properties of the homemade electrocatalysts, which were mixed with Nafion® solution and cast on a glassy carbon disk electrode (5 mm OD) mounted in an interchangeable RDE holder (Pine Instruments), were examined in 0.5 M $HClO_4$ aqueous solution at 25 °C. The electrocatalyst layer on RDE was prepared by casting 7 μl of electrocatalyst slurry obtained by mixing 10 mg electrocatalysts (Pt/C or $Co_{rich\ core}$-$Pt_{rich\ shell}$/C), 100 μl Nafion® solution (5 wt.%, Du Pont) and 500 μl DI water, respectively. The Pt electroactive areas of electrocatalysts were measured by the cyclic voltammetry (CV) with the scan range and rate of 0.05–1.2 V and 50 mV s^{-1} in 0.5 M $HClO_4$ under N_2 atmosphere. The linear sweep voltammetry (LSV) on hydrodynamic RDE with the rotating rate of 400–2000 rpm was performed at the scan rate of 0.5 mV s^{-1}. The gas with a suitable partial pressure of O_2 was first sparged at 40 ml min^{-1} into the electrolyte for 30 min, and then kept flowing above the electrolyte during the ORR measurements.

3. Results and discussion

3.1. Characterization of Pt/C and $Co_{rich\ core}$-$Pt_{rich\ shell}$/C

The good dispersion of Pt and $Co_{rich\ core}$-$Pt_{rich\ shell}$ particles on the carbon support was found in TEM images as shown in Figs. 1(a) and 2(a). The particle sizes of Pt and $Co_{rich\ core}$-$Pt_{rich\ shell}$ on the support were found to be 2–5 and 3–6 nm, and their mean particle sizes estimated according to Figs. 1(b) and 2(b) were 3.58 and 4.12 nm, respectively. The Co core covered with Pt shell resulted in the greater particle size of $Co_{rich\ core}$-$Pt_{rich\ shell}$ than that of Pt.

The peaks of XRD patterns of Pt/C and $Co_{rich\ core}$-$Pt_{rich\ shell}$/C at 2θ of 39.79, 46.28, 67.53, 81.34 and 85.79° corresponded to the crystal planes of (1 1 1), (2 0 0), (2 2 0), (3 1 1) and (2 2 2) represented the fcc structure of Pt as illustrated in Fig. 3. The grain size, Pt–Pt interatomic distance and lattice parameter of the Pt/C estimated by the Scherrer's equation [11] based on the crystal face of (1 1 1) (2θ = 39.79°) were 3.06 ± 0.014, 0.227, and 0.3920 nm, respectively. As shown in Table 1, similar results were obtained for $Co_{rich\ core}$-$Pt_{rich\ shell}$/C electrocatalyst. However, the Pt grain

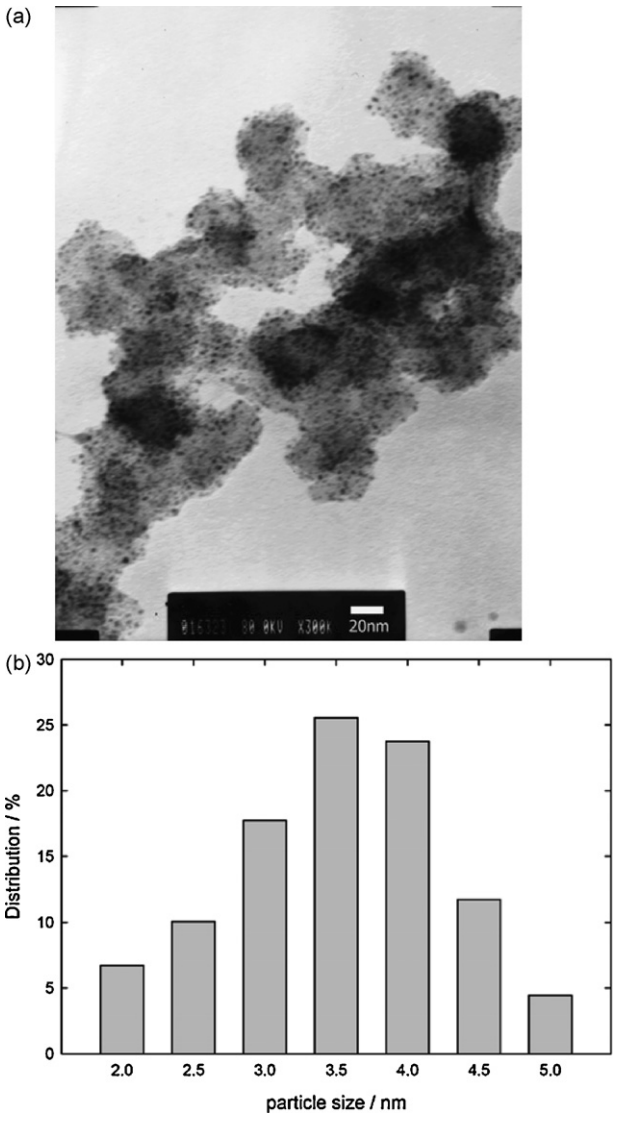

Fig. 1. (a) TEM photographs and (b) particle size distribution of Pt/C.

size of $Co_{rich\ core}$-$Pt_{rich\ shell}$/C obtained to be 3.17 ± 0.009 nm was slightly greater than that of Pt/C. The results in Fig. 3 also revealed that the Pt diffraction peaks of $Co_{rich\ core}$-$Pt_{rich\ shell}$/C were slightly shifted to higher 2θ values in comparison with Pt/C. The shift in Pt (1 1 1) diffraction peak from 39.79° (Pt/C) to a higher value of 40.05° ($Co_{rich\ core}$-$Pt_{rich\ shell}$/C) (Table 1) was deduced to the incorporation of Co into the Pt fcc structure. The Pt–Pt interatomic distance and lattice parameter of $Co_{rich\ core}$-$Pt_{rich\ shell}$/C were 0.225 and 0.3878 nm, respectively. Based on the shift in diffraction angle and the change in Pt lattice parameter, the alloying degree of the $Co_{rich\ core}$-$Pt_{rich\ shell}$ was calculated according to Vegard's law [12] to be 14.75% (Table 1). The low alloying degree and absence of the Co diffraction peaks in the XRD pattern indicated that the structure

Table 1
Crystal structure characteristics of Pt/C and $Co_{rich\ core}$-$Pt_{rich\ shell}$/C.

Catalysts	2θ of Pt (1 1 1) (°)	Grain size[a] (nm)	Pt–Pt interatomic distance (nm)	Lattice parameter (nm)	Degree of alloying (%)
Pt/C	39.79	3.06 ± 0.014	0.227	0.3920	–
$Co_{rich\ core}$-$Pt_{rich\ shell}$/C	40.05	3.17 ± 0.009	0.225	0.3878	14.75

Conditions for preparing electrocatalysts: Pt/C: 100 mg XC-72, 10 ml dpe solution with composition of [$Pt(acac)_2$]: [1,2-hexadecandiol] = 12.72 mM: 38.69 mM, $Co_{rich\ core}$-$Pt_{rich\ shell}$/C: 200 mg XC-72, 20 ml dpe solution with composition of [$Co_2(CO)_8$]: [$Pt(acac)_2$]: [1,2-hexadecandiol] = 14.57 mM:12.72 mM:38.69 mM.

[a] The grain sizes were calculated based on the crystal face of Pt (1 1 1) from XRD.

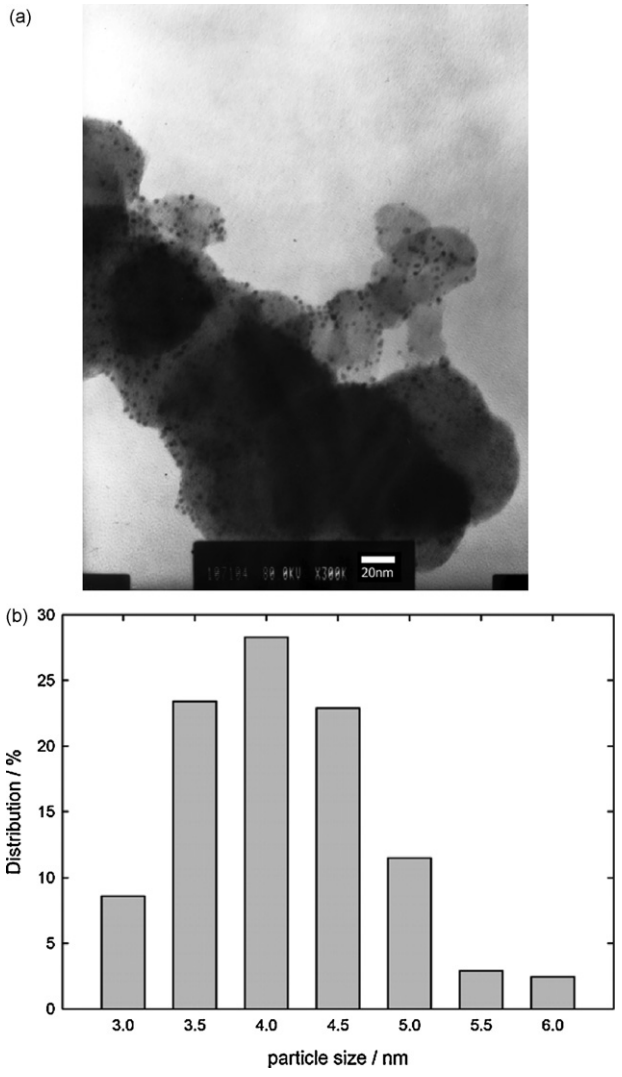

Fig. 2. (a) TEM photographs and (b) particle size distribution of $Co_{rich\ core}$-$Pt_{rich\ shell}$/C.

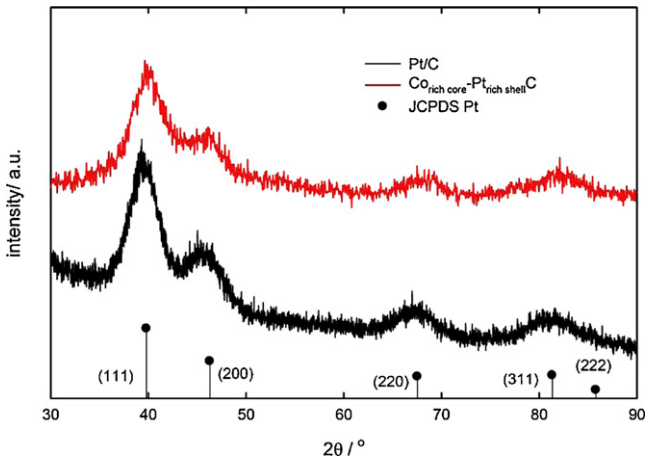

Fig. 3. XRD spectras of Pt/C and $Co_{rich\ core}$-$Pt_{rich\ shell}$/C.

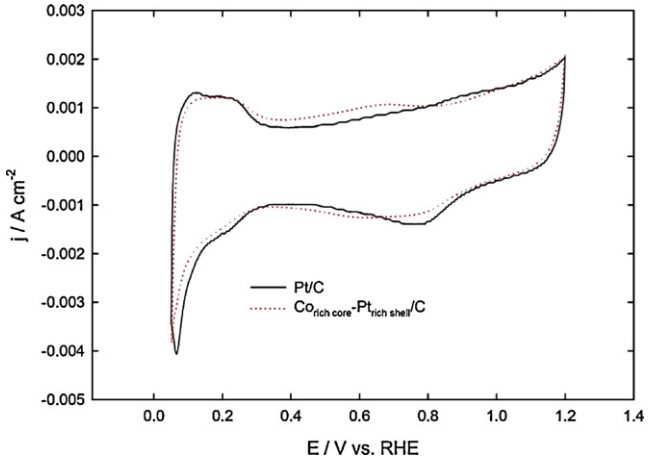

Fig. 4. Cyclic voltammograms of Pt/C and $Co_{rich\ core}$-$Pt_{rich\ shell}$/C in 0.5 M $HClO_4$. WE: Pt/C, geometric area of WE = 0.196 cm^{-2}, RE: RHE (0.5 M $HClO_4$), CE: Pt foil, temperature = 25 ± 0.5 °C, scan rate: 50 mV s^{-1}, scan range = 0.05–1.2 V, N_2 flow rate = 40 ml min^{-1} for 30 min.

of $Co_{rich\ core}$-$Pt_{rich\ shell}$ was near the Pt shell covered on the relative small Co core.

3.2. *Electrochemical properties of Pt/C and $Co_{rich\ core}$-$Pt_{rich\ shell}$/C*

Using Pt/C and $Co_{rich\ core}$-$Pt_{rich\ shell}$/C as the cathodic electrocatalysts, the similar cyclic voltammograms in 0.5 M $HClO_4$ aqueous solution under N_2 atmosphere were found in Fig. 4. The cathodic and anodic peaks located in the potential range of 0.05–0.4 V were caused by the reduction of proton and the hydrogen desorption, respectively. The formation and reduction of oxides were found for the potentials greater than 0.6 V. The Pt electroactive areas of Pt/C and $Co_{rich\ core}$-$Pt_{rich\ shell}$/C evaluated according to the charges for oxidizing hydrogen adsorbed on Pt surface were 44.16 and 37.50 $m^2\ g^{-1}$, respectively. The LSV of ORR on Pt/C and $Co_{rich\ core}$-$Pt_{rich\ shell}$/C in the oxygen saturated 0.5 M $HClO_4$ aqueous solution with various rotating rates at 25 °C were illustrated in Figs. 5(a) and 6(a). The results indicated that the ORR was controlled by the diffusion of dissolved oxygen from bulk solution to the electrode surface when the potential was less than 0.7 V. The limiting current densities of ORR were progressively increased with the rotating rate due to the increase in the mass transfer rate of the dissolved oxygen. For the potential in the range of 0.7–0.85 V, the ORR was under the diffusion-kinetic mixing control.

The current density, mass activity (MA) and specific activity (SA) of ORR in 0.5 M $HClO_4$ saturated with O_2 were evaluated at the kinetic control region, i.e. the potential greater than 0.85 V in Figs. 5(a) and 6(a). Compared with Pt/C the greater current density, MA and SA of ORR on $Co_{rich\ core}$-$Pt_{rich\ shell}$/C at η = 0.1 V (Table 2) revealed that the electroactivity of ORR on $Co_{rich\ core}$-$Pt_{rich\ shell}$/C was greater than that on Pt/C. The overpotential (η) of the electrocatalytic ORR was defined as the difference between the applied potential and the open circuit potential (OCP). The OCPs of ORR on the Pt/C and $Co_{rich\ core}$-$Pt_{rich\ shell}$/C were experimentally found to be 0.97 and 0.98 V, respectively. The MA and SA of ORR on $Co_{rich\ core}$-$Pt_{rich\ shell}$/C

Table 2
The electrochemical characteristics of ORR on Pt/C and $Co_{rich\ core}$-$Pt_{rich\ shell}$/C.

Electrocatalyst	cd[a] (A cm^{-2})	MA[b] (A g^{-1})	SA[c] (A cm^{-2})
Pt/C	2.83×10^{-4}	6.69	1.51×10^{-5}
$Co_{rich\ core}$-$Pt_{rich\ shell}$/C	4.11×10^{-4}	10.22	2.73×10^{-5}

WE: Pt/C or $Co_{rich\ core}$-$Pt_{rich\ shell}$/C, geometric area of WE = 0.196 cm^{-2}, RE: RHE (0.5 M $HClO_4$), CE: Pt foil, electrolyte: 0.5 M $HClO_4$ saturated with O_2, temperature = 25 ± 0.5 °C, scan rate: 0.5 mV s^{-1}, scan range = 0.4–1.05 V, O_2 flow rate = 40 ml min^{-1} for 30 min.

[a] Current density of ORR at overpotential of 0.1 V.
[b] Mass activity of ORR at overpotential of 0.1 V.
[c] Specific activity of ORR at overpotential of 0.1 V.

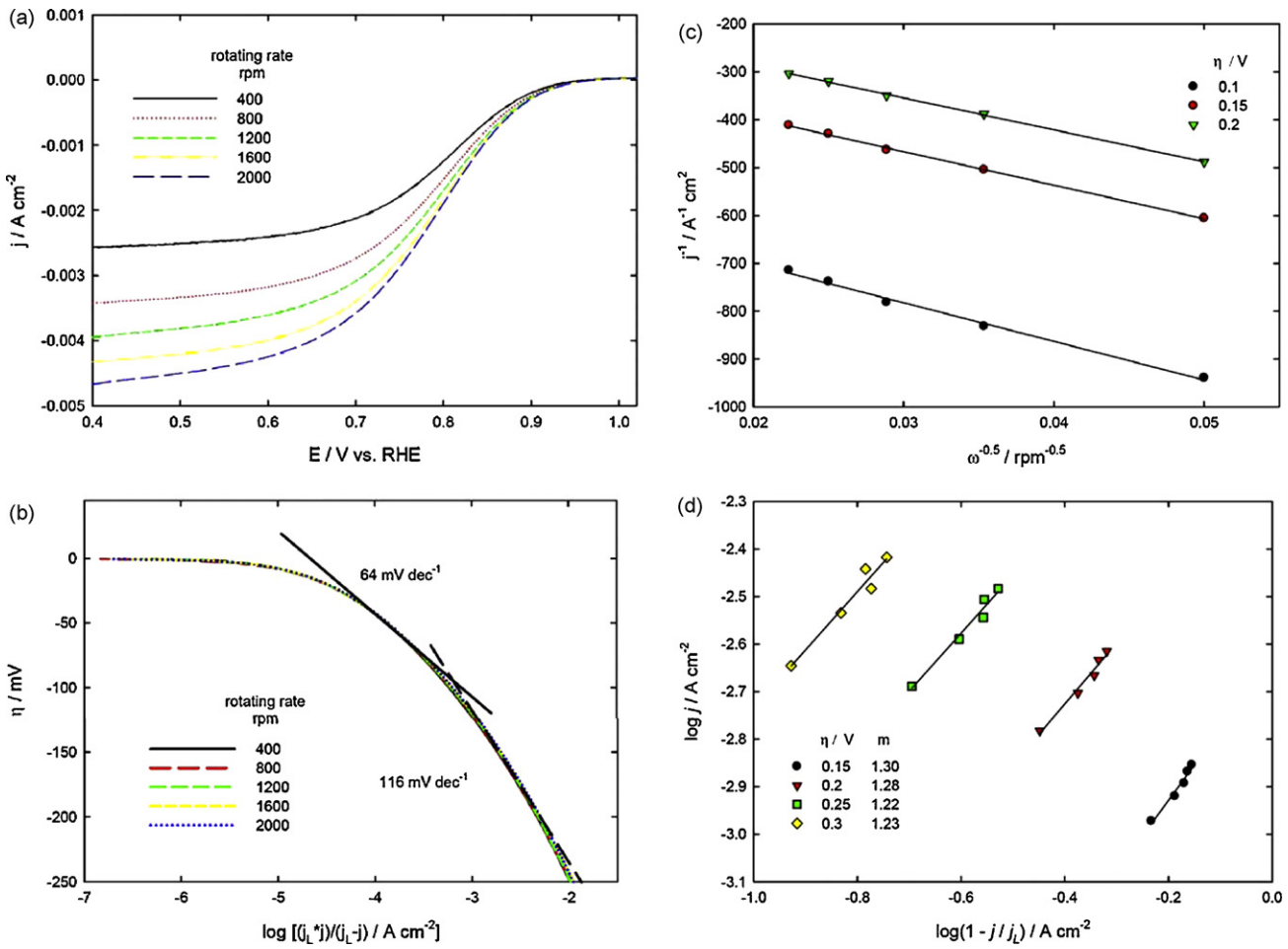

Fig. 5. (a) Linear scan voltammograms, (b) mass transport corrected Tafel plots, (c) Levich–Koutecky plots and (d) dependence $\log(j)$ versus $\log(1-j/j_L)$ for ORR on Pt/C in oxygen saturated 0.5 M $HClO_4$ with various rotating rates. WE: Pt/C, geometric area of WE = 0.196 cm^{-2}, RE: RHE (0.5 M $HClO_4$), CE: Pt foil, electrolyte: 0.5 M $HClO_4$ saturated with O_2, temperature = 25 ± 0.5 °C, scan rate: 0.5 mV s^{-1}, scan range = 0.4–1.05 V, O_2 flow rate = 40 ml min^{-1} for 30 min.

were 1.5 and 1.8 folds for that on Pt/C. The higher electroactivity of ORR on $Co_{rich\ core}$-$Pt_{rich\ shell}$/C was deduced to be the shorter Pt–Pt interatomic distance (Table 1) and the electronic effect caused by the presence of Co. It is known that the enhancement in the ORR activity on Pt based alloy catalysts is generally correlated to the change in Pt–Pt interatomic distance [1]. Thus, it was believed that the Pt–Pt interatomic distance played an important role in the electrocatalysis of ORR.

3.3. Kinetics of ORR on Pt/C and $Co_{rich\ core}$-$Pt_{rich\ shell}$/C

The ORR could be divided into the kinetic, mixed and mass transfer controlled regions with the potentials greater than 0.85 V, located within 0.85–0.7 V and less than 0.7 V as indicated in the LSV curves (Figs. 5(a) and 6(a)). Two Tafel slopes of 64 and 116 mV dec^{-1} at a relative lower η (50–100 mV) and a higher η (120–200 mV) mV were obtained from the almost overlapped mass transport corrected Tafel plots of ORR on Pt/C with various rotating rates (Fig. 5(b)). Similar results were also obtained for ORR on $Co_{rich\ core}$-$Pt_{rich\ shell}$/C with two Tafel slopes of 67 and 110 mV dec^{-1} at the lower and higher η as shown in Fig. 6(b). The small Tafel slope (~60 mV dec^{-1}) on the electrocatalysts at a relative lower η might be due to the formation of Pt oxides and/or the adsorption of OH species on the electrode surface [13]. For the overpotential greater than 120 mV, the reduction of oxides and/or the desorption of OH species existed on the surface of electrocatalysts resulted in an increase in the Tafel slope to a higher value (~120 mV dec^{-1}). Damjanovic et al. [14,15] proposed that the small Tafel slope of ORR at the low overpotential region (<100 mV) might be caused by the oxygen reduction on an oxide-covered Pt surface, and the higher Tafel slope at the high overpotential region (>120 mV) was due to the low coverage of oxygen-containing species on the electrode surface. The exchange current densities of ORR on Pt/C and $Co_{rich\ core}$-$Pt_{rich\ shell}$/C determined based on the higher Tafel slope were found to be 6.76×10^{-5} and 9.21×10^{-5} A cm^{-2}, respectively, at 25 °C. The experimental results implicated that the fast ORR kinetic would be obtained on $Co_{rich\ core}$-$Pt_{rich\ shell}$/C rather than Pt/C. However, based on the similar Tafel slopes of ORR on both Pt/C and $Co_{rich\ core}$-$Pt_{rich\ shell}$/C suggested that they had the same ORR reaction mechanisms.

Figs. 5(c) and 6(c) represented the inverse current densities of ORR (j^{-1}) on Pt/C and $Co_{rich\ core}$-$Pt_{rich\ shell}$/C as a function of the inverse of the square root of rotating rate ($\omega^{-0.5}$) at various overpotentials, the so-called Levich–Koutecky plots. In a film-coated electrode surface, the overall current density (j) was related to the kinetic current density (j_k), the liquid film diffusion-limited current density (j_d), and the Nafion® film diffusion-limited current (j_f) as shown in Eq. (1). The effect of the Nafion® film diffusion could be neglected in the present condition since the mass ratio of Nafion® and the electrocatalyst (1.15 μl 5 wt.% Nafion® in 7 μl of slurry) within the film-type electrode was sufficiently small, that is, the small diffusion resistance through the Nafion® film [13,16]. Thus, the overall measuring current density of ORR could be written as depending on the kinetic current density and the diffusion

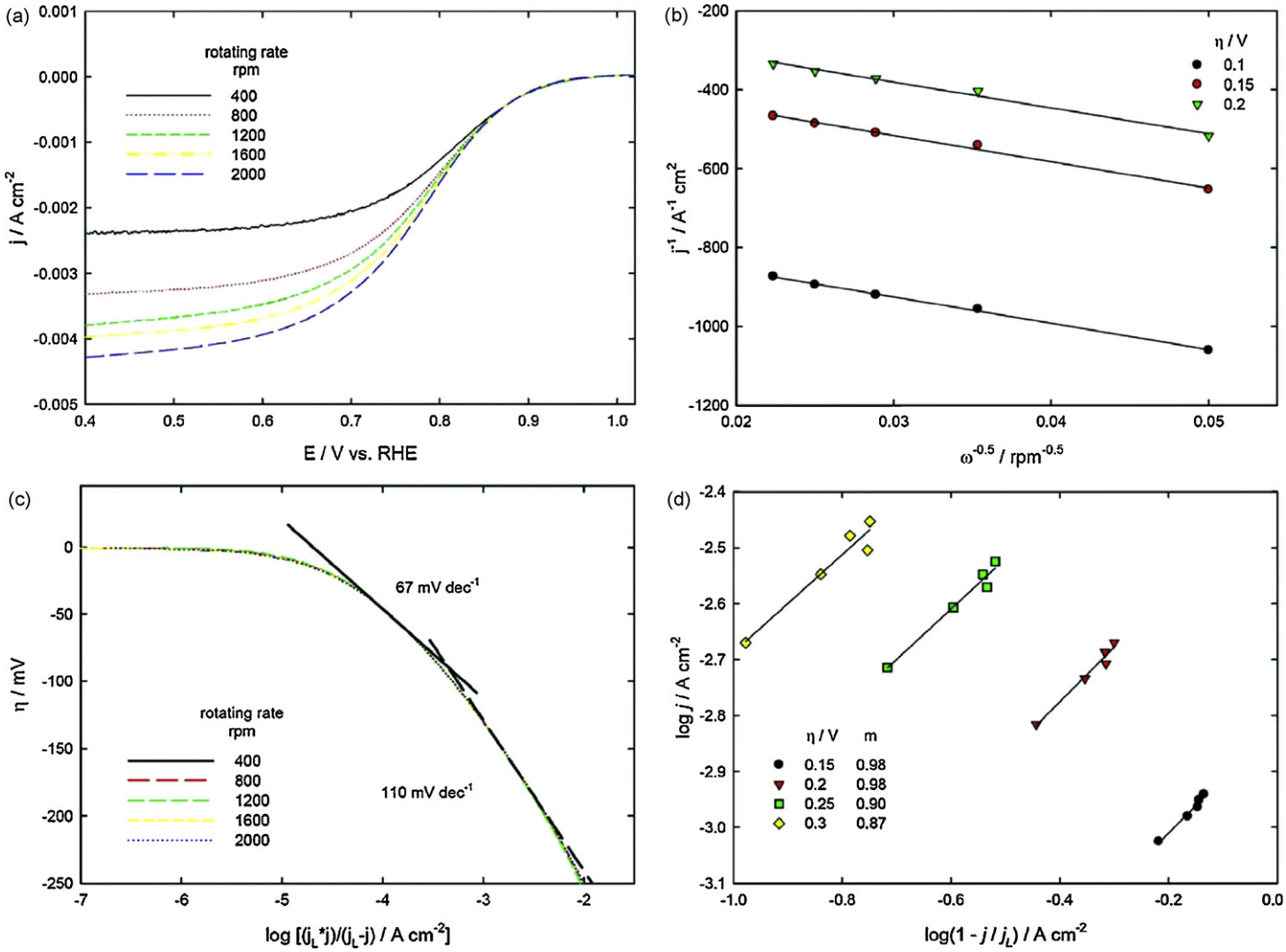

Fig. 6. (a) Linear scan voltammograms (b) mass transport corrected Tafel plots (c) Levich–Koutecky plots (d) dependence log(j) versus log($1-j/j_L$) for ORR on $Co_{rich\ core}$-$Pt_{rich\ shell}$/C in oxygen saturated 0.5 M $HClO_4$ with various rotating rates. WE: $Co_{rich\ core}$-$Pt_{rich\ shell}$/C, geometric area of WE = 0.196 cm^{-2}, RE: RHE (0.5 M $HClO_4$), CE: Pt foil, electrolyte: 0.5 M $HClO_4$ saturated with O_2, temperature = 25 ± 0.5 °C, scan rate: 0.5 mV s^{-1}, scan range = 0.4–1.05 V, O_2 flow rate = 40 ml min^{-1} for 30 min.

current density through the liquid film as shown in Eq. (1),

$$\frac{1}{j} = \frac{1}{j_k} + \frac{1}{j_d} + \frac{1}{j_f} = \frac{1}{j_k} + \frac{1}{B\omega^{1/2}} \quad (1)$$

The inverse of slope of the linear relationship between j^{-1} and $\omega^{-1/2}$, the so-called B factor, was equal to $0.62nFC_OD^{2/3}\nu^{-1/6}$ where n was the electron transfer number, F was the Faraday constant (96,485 coul mol^{-1}), D was the diffusivity of O_2 in the electrolyte (1.9×10^{-9} m^2 s^{-1} [17]), C_O was the O_2 concentration in the solution (0.969 mM measured by a dissolved oxygen (DO) meter), ν was the kinetic viscosity (0.893×10^{-2} cm^2 s^{-1} [18]), and ω was the rotating rate of RDE. The slopes by plotting j^{-1} against $\omega^{-1/2}$ on Pt/C and $Co_{rich\ core}$-$Pt_{rich\ shell}$/C electrocatalysts were found from Figs. 5(c) and 6(c) to be 7.24 ± 0.73 and 6.63 ± 0.07 A^{-1} cm^2 $rpm^{0.5}$, respectively. The electron transfer numbers calculated based the slopes (B^{-1}) in Figs. 5(c) and 6(c) were equal to 4 for both of the electrocatalysts, indicating the ORR on both Pt/C and $Co_{rich\ core}$-$Pt_{rich\ shell}$/C at various overpotentials followed a four-electron path to produce water.

One of the most extensively studied electrochemical reactions is the four-electron electroreduction of oxygen to water in acid solution (Eq. (2)) [1]:

$$O_2 + 4H^+ + 4e \rightarrow 2H_2O \quad (2)$$

The reaction rate of the oxygen reduction with respect to the dissolved oxygen and the proton in the solution could be expressed as,

$$r = \frac{j}{nFA} = kC_{s,O}^{m}C_{H^+}^{p} \quad (3)$$

where k was the rate constant, $C_{s,O}$ was the concentration of O_2 at the surface of rotating electrode, C_{H^+} was the concentration of H^+ in the solution, j was the disc current density, and m and p were the reaction orders with respected to the dissolved oxygen and H^+, respectively. The concentration of oxygen on the electrode surface ($C_{s,O}$) could be expressed as $(1-j/j_L)C_O$ [19,20], where j_L was the limiting current of ORR. Based on the constant concentration of H^+ for a fixed pH of solution, the Eq. (4) could be expressed as,

$$r = \frac{j}{nFA} = k'\left[\left(1-\frac{j}{j_L}\right)C_O\right]^m \quad (4)$$

where k' was equal to $kC_{H^+}^{p}$. According to Eq. (4), the reaction order of dissolved oxygen could be determined by plotting log(j) versus log($1-j/j_L$) at various rotating rates as the following equation [20],

$$\log j = \log j_k + m\log\left(1-\frac{j}{j_L}\right) \quad (5)$$

where j_k was the kinetic current density ($j_k = nFAk'C_O^m$). Eq. (5) can be only employed for the reaction under kinetic–diffusion

mixed control region. The plots of $\log(j)$ versus $\log(1 - j/j_L)$ as shown in Figs. 5(d) and 6(d) for ORR on Pt/C and $Co_{rich\ core}$-$Pt_{rich\ shell}$/C resulted in the straight lines. The slopes of the straight lines obtained to be 0.87–1.3 for the overpotentials of 0.15–0.3 V implied a first order reaction of oxygen on both Pt/C and $Co_{rich\ core}$-$Pt_{rich\ shell}$/C electrocatalysts.

4. Conclusions

The characteristics and the electrochemical kinetics of the nano-sized Pt/C and $Co_{rich\ core}$-$Pt_{rich\ shell}$/C prepared by combining the chemical reduction and the thermal decomposition methods were investigated. The same fcc crystal structure of Pt/C and $Co_{rich\ core}$-$Pt_{rich\ shell}$/C were demonstrated by the XRD, and their mean particle sizes based on TEM analysis were 3.58 and 4.12 nm, respectively. The MA and SA of ORR on $Co_{rich\ core}$-$Pt_{rich\ shell}$/C electrocatalyst were obtained to be 10.22 A g^{-1} and 2.73×10^{-5} A cm^{-2}, which were 1.5 and 1.8 times of ORR on Pt/C. The increase in the electroactivity of ORR on $Co_{rich\ core}$-$Pt_{rich\ shell}$/C was ascribed to be the decrease in the Pt–Pt mean interatomic distance and the electronic effect caused by the presence of Co. The kinetics of the ORR on both of the homemade Pt/C and $Co_{rich\ core}$-$Pt_{rich\ shell}$/C electrocatalysts in 0.5 M $HClO_4$ aqueous solution were examined by the film-type electrocatalysts on RDE. Two Tafel slopes were experimentally obtained to be 67 and 110 mV dec^{-1} at the overpotential less than 100 mV and greater than 120 mV for $Co_{rich\ core}$-$Pt_{rich\ shell}$/C. The similar Tafel slopes of ORR were obtained by using Pt/C as the electrocatalyst. The exchange current density of ORR on $Co_{rich\ core}$-$Pt_{rich\ shell}$/C was obtained to be 9.21×10^{-5} A cm^{-2}, which was significantly greater than that on Pt/C (6.76×10^{-5} A cm^{-2}). The ORR on both Pt/C and $Co_{rich\ core}$-$Pt_{rich\ shell}$/C following a four electron reaction mechanism was demonstrated by the experimental data and kinetic studies.

Acknowledgments

The financial support of the National Science Council Republic of China (Project number: NSC 96-2120-M-011-001) and Tunghai University is gratefully acknowledged.

References

[1] L. Carrette, K.A. Friedrich, U. Stimming, Fuel Cells 1 (2001) 5–39.
[2] T. Toda, H. Igarashi, H. Uchida, M. Watanabe, J. Electrochem. Soc. 146 (1999) 3750–3756.
[3] J. Shim, D.Y. Yoo, J.S. Lee, Electrochim. Acta 45 (2000) 1943–1951.
[4] M.K. Min, J. Cho, K. Cho, H. Kim, Electrochim. Acta 45 (2000) 4211–4217.
[5] S. Koh, C. Yu, P. Mani, R. Srivastava, P. Strasser, J. Power Source 172 (2007) 50–56.
[6] M. Watanabe, K. Tsurumi, T. Mizukami, T. Nakamura, P. Stonehart, J. Electrochem. Soc. 141 (1994) 2659–2668.
[7] N. Wakabayashi, M. Takeichi, H. Uchida, M. Watanabe, J. Phys. Chem. B 109 (2005) 5836–5841.
[8] H.R. Colón-Mercado, H. Kim, B.N. Popov, Electrochem. Commun. 6 (2004) 795–799.
[9] R.R. Adžić, J.X. Wang, Electrochim. Acta 45 (2000) 4203–4210.
[10] J.S. Do, Y.T. Chen, M.H. Lee, J. Power Sources 172 (2007) 623–632.
[11] W. Li, W. Zhou, H. Li, Z. Zhou, B. Zhou, Electrochim. Acta 49 (2004) 1045–1055.
[12] J.R.C. Salgado, E. Antolini, E.R. Gonzalez, J. Power Sources 138 (2004) 56–60.
[13] V.S. Murthi, R.C. Urian, S. Mukerjee, J. Phys. Chem. B 108 (2004) 11011–11023.
[14] A. Damjanovic, V. Brusic, Electrochim. Acta 12 (1967) 615–628.
[15] A. Damjanovic, M.A. Genshaw, Electrochim. Acta 15 (1970) 1281–1283.
[16] K. Súarez-Alćantara, A. Rodŕıguez-Castellanos, R. Dante, O. Solorza-Feria, J. Power Sources 157 (2006) 114–120.
[17] R.R. Adžić, J. Wang, B.M. Ocko, Electrochim. Acta 40 (1995) 83–89.
[18] K.E. Gubbins, R.D. Walker Jr., J. Electrochem. Soc. 112 (1965) 469–471.
[19] A.J. Bard, L.R. Faulkner, Electrochemical Methods: Fundamentals and Applications, second ed., John Wiley & Sons, New York, 2001, pp. 340–341.
[20] C.C. Chang, T.C. Wen, H.J. Tien, Electrochim. Acta 42 (1997) 557–565.